Impact of mismatch-related phenomena on a room-temperature operation of nitride VCSELs

Paweł Maćkowiak, Włodzimierz Nakwaski*

Institute of Physics, Technical University of Łódź, ul. Wólczańska 219, 93–005 Łódź, Poland.

The influence of mismatch-related phenomena (mostly strain fields and structure defects) on a room- temperature (RT) operation of possible nitride VCSELs is examined using a simple but still detailed analytical model. Intentionally introduced stress fields within nitride VCSEL quantum-well (QW) active regions (band-gap engineering) are found to have a much weaker effect on their optical gain than in the case of conventional arsenide and phosphide VCSELs. Dislocation densities (including misfit dislocations), on the other hand, have a considerable harmful impact on VCSELs thresholds, mostly because of increasing scattering losses and decreasing internal quantum efficiency. Single-quantum-well nitride VCSELs are found to be very sensitive to the above impact. A reasonable increase in a number of QWs in multiple-quantum-well VCSELs tremendously improves their performance. In the case of relatively high dislocation densities, bulk double-heterostructure VCSELs may turn out to be the best nitride designs although they may also exhibit too high thresholds to lase at RT.

1. Introduction

Nowadays, short-wavelength (ultra-violet and blue) light emitting nitride semiconductor lasers based on wide-gap GaN, AlN, and InN semiconductor materials and their solid solutions [1] attract considerable attention. This is due to possible wide applications of these lasers in high-density optical recording devices [2], *i.e.*, in CD players, video-disk recorders, optical computer memory systems, *etc.*, as well as in printing and imaging devices. First room-temperature (RT) operation of nitride edge-emitting lasers (EELs) was reported by NAKAMURA *et al.* [3] in 1996. However, there have been only a few successful attempts to produce optically pumped nitride vertical-cavity surface-emitting lasers (VCSELs) [4], [5] and no electrically-pumped nitride VCSELs have been reported until now. Nevertheless, because of their unique anticipated performance properties [6], VCSELs are believed to be an inevitable future of nitride lasers.

Conventional arsenide and phosphide VCSEL designs are usually complex structures manufactured from very many layers of different composition, *i.e.*, different lattice constants. This is followed by some mismatch-related phenomena. Designs of nitride VCSELs are believed to have similarly complex structures. Therefore an

---

*Also with the Center for High Technology Materials, University of New Mexico, Albuquerque, NM 87131, USA.

analysis of the influence of the above phenomena on a possible RT operation of nitride VCSELs could be helpful in optimizing their configurations. Such an analysis is given in the present paper, which is organized as follows. The VCSEL structure under consideration is explained in Sec. 2. The model used to simulate RT-operation of nitride VCSELs is presented shortly in Sec. 3. Section 4 is devoted to mismatch-related phenomena. Results of our modelling are presented in Sec. 5, which is followed by conclusions.

2. Structure

For the analysis, the GaN/AlGaN/AlN VCSEL structure has been intentionally chosen because it could extend the range of semiconductor diode lasers deep into the UV. Until now many UV light-emitting diodes of analogous structures have already been reported [7]−[10]. However, it should be stressed that standard In-GaN/AlGaN/GaN laser structures exhibit much lower thresholds because their simulated recombination takes place between carriers localized by large potential fluctuations in the InGaN layers (quantum-dot-like structures) due to difficulties in uniform In incorporation. Unfortunately, analogous potential fluctuations in the AlGaN layers are not expected to provide similar recombination mechanism [11].

It is well known that manufacturing high-quality (at least free from cracks) epitaxial nitride films is more difficult than producing other $A^{III}B^{V}$ materials. The reason for that is mostly associated with relatively high differences in lattice constants between commonly used substrate materials (SiC, Al_2O_3, GaAs, Si and others) and nitride layers. At present, this situation seems to have been finally radically improved because "perfect" GaN substrates become available [12]−[16]. Nevertheless, even in the case of previous substrate materials, the surface morphology of grown nitride films can be considerably improved by using GaN, AlN or (AlGa)N buffer layers [7], [17]−[22]. Buffer layers are supposed to convey the
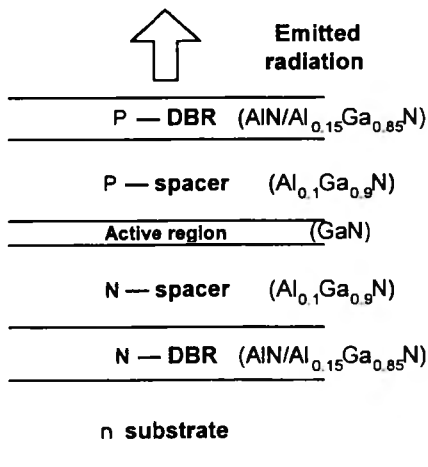

Fig. 1. Schematic structure of a nitride top-emitting vertical cavity surface emitting laser (VCSEL).

information of the substrate crystallographic structure, such as its orientation, but additionally to relax strains produced during this heteroepitaxial growth. Therefore thick (even up to 2.5 µm) low-AlN-content AlGaN layers [9] as well as somewhat thinner (0.4 µm) high-Al-content AlGaN layers [23] of good quality have already been reported. Attempts to grow thick (more than 0.6 µm) AlGaN layers with more than 8% Al content have sometimes resulted in formation of defective structures with cracked surfaces [9], [10]. However, it seems to be relatively easy to produce good-quality 0.4-µm $Al_{0.1}Ga_{0.9}N$ cladding layers which ensure almost perfect carrier confinement [24].

On the basis of the above discussion, the analysis is carried out for a top-emitting VCSEL structure schematically shown in Fig. 1. Three types of GaN active regions are taken into consideration: bulk GaN double-heterostructure (DH) active region, as well as single-quantum-well (SQW) and the multiple-quantum-well (MQW) $GaN/Al_{0.2}Ga_{0.8}N$ active regions. Both (P-type and N-type) spacers are assumed to be manufactured from $Al_{0.1}Ga_{0.9}N$ and both distributed Bragg reflector (DBR) resonator mirrors — from $AlN/Al_{0.15}Ga_{0.85}N$ stacks.

3. Model

The lasing threshold condition for diode lasers may be expressed as [25]

$$\Gamma_A g_{th} = \alpha_i + \alpha_{end} \tag{1}$$

with the internal (α_i) and the end (α_{end}) loss coefficients:

$$\alpha_i = \Gamma_A \alpha_A + \Gamma_P \alpha_P + \Gamma_N \alpha_N + \alpha_{diff} + \alpha_{scatt}, \tag{2}$$

$$\alpha_{end} = \frac{1}{2L} \ln\left(\frac{1}{R_F R_R}\right) \tag{3}$$

where (for K = A (active layer), P (P-type spacer), N (N-type spacer)) $\Gamma_K = d_K/L$ stand for the confinement factors within corresponding layers (assuming uniform field distribution between resonator mirrors), d_K are their thicknesses (cumulative thickness in the case of a MQW active region) and α_K are loss coefficients in corresponding layers, respectively. L is the resonator length (including penetration depths) R_F and R_R are the reflectivities of the front and the rear resonator mirrors [26], respectively, and $g_{th} \equiv g(n = n_{th})$ is the threshold gain achieved for the carrier concentration n equal to its threshold value n_{th}. In the simulation, energy penetration depths are determined with the aid of the approach given in [27], material losses ($\alpha_m = 10$ cm^{-1}) associated mainly with the band-to-band absorption via the states localized in deep band tails are found in [28], and free-carrier losses ($\alpha_{fc} = 1$ cm^{-1}) are extracted from data reported in [29]. Active-region losses are assumed to be mainly free-carrier absorption ($\alpha_A = \alpha_{fc,A}$), whereas optical losses in spacers contain also material losses ($\alpha_P = \alpha_{fc,P} + \alpha_{m,P}$ and $\alpha_N = \alpha_{fc,N} + \alpha_{m,N}$). Scattering losses ($\alpha_{scatt} = 5$ cm^{-1}) are calculated on the basis of [30] and diffraction losses (α_{diff}) are assumed to be negligible in index-guided (IG) VCSELs ($\alpha_{difft} = 0$), whereas for gain-guided

(GG) VCSELs they are determined using an approach proposed by BABIĆ *et al.* [31] (see Fig. 4 therein).

The maximum optical gain may be written as

$$g(n) = \begin{cases} a(n-n_{tr,b}) & \text{for bulk active regions,} \\ b\ln(n/n_{tr,QW}) & \text{for QW active regions} \end{cases} \tag{4}$$

where [32], [33]: $a = 2.5 \cdot 10^{-16}$ cm^{-2}, $n_{tr,b} = 7.5 \cdot 10^{18}$ cm^{-3} for DH active regions ($d_A = 0.2$ μm), and [34]: $b = 7.22 \cdot 10^3$ cm^{-1} and $n_{tr,QW} = 1.17 \cdot 10^{19}$ cm^{-3} for strained GaN/Al$_{0.2}$Ga$_{0.8}$N quantum wells ($d_A = 4$ nm), *cf.* Sec. 4.1.

The threshold current density j_{th} may be directly related to the threshold carrier concentration n_{th} with the aid of the following relation:

$$j_{th} = \left(\frac{ed_A}{\eta_i}\right)(An_{th} + Bn_{th}^2 + Cn_{th}^3) \tag{5}$$

where e is the electron charge, $A = 1 \cdot 10^8$ s^{-1}, $B = 1.5 \cdot 10^{-11}$ cm^3 s^{-1}, and $C = 1.4 \cdot 10^{-31}$ cm^6 s^{-1} and η_i is the internal quantum efficiency, calculated following the approach of SUGAHARA *et al.* [35] (*cf.* Sec. 4.2). More details about the model may be found in our previous papers [36]−[38].

4. Mismatch-related phenomena

In manufacturing conventional GaAs/AlGaAs and InGaAsP/InP diode lasers, either the lattice-matched or the strained lattice-mismatched structures are used. In both cases, however, coherence of the growth is rigorously preserved. Continuum elasticity theory predicts that for small lattice misfits f defined as

$$f = 1 - \frac{a_{epi}}{a_{sub}} \tag{6}$$

(where a_{epi} and a_{sub} stand for lattice constants of the deposit (epi) and the substrate (sub), respectively) initially a pseudomorphic crystal growth is observed [39]. An increase in the epi-layer thickness, however, is followed by a corresponding increase in an elastic strain at the heteroboundary until it is sufficient to activate a misfit dislocation. Then such a dislocation is created and plastic relaxation occurs. Also other defects can play an important role for this strain relief. This critical thickness d_{cr} depends on both heterostructure components and is a function of f.

4.1. Quantum-well nitride active regions

For the GaN/Al$_{0.1}$Ga$_{0.9}$N heterostructure, d_{cr} is somewhat lower than 100 nm, decreasing to about 40 nm for the GaN/Al$_{0.2}$Ga$_{0.8}$N heterostructure [40]. Accordingly, in standard GaN/AlGaN quantum wells, a lattice mismatch is accomodated by internal strains rather than by the formation of misfit dislocations. In a typical 6-nm GaN/Al$_{0.2}$Ga$_{0.8}$N QW, for example, the GaN layer is compressively strained by a lattice mismatch of -0.5% [34], [41]. In conventional (*e.g.*, arsenide and

phosphide) zincblende $A^{III}B^{V}$ heterostructure diode lasers, such a biaxial strain is intentionally used to reduce their threshold currents (band-gap engineering). Because of the hexagonal crystal symmetry of wurtzite nitrides and their small spin-orbit coupling, however, this effect has been found by SUZUKI and UENOYAMA [34], [42] to be much smaller in nitride heterostructure diode lasers, so their thresholds are only slightly reduced (see Fig. 4 in [34]). Nevertheless, strain influence on optical gain is included in our simulation concerning QW nitride VCSELs (Eq. (4)).

There is also another consequence of stress fields in QW nitride structures. Nitrides exhibit strongly pronounced piezoelectric properties [43]–[46]. Therefore, strains induced in nitride structures by the lattice mismatch generate the electric field perpendicular to the QW layer edges pulling electrons and holes in opposite directions [47]–[49]. This may affect band-edge absorption near the exciton peak reducing energies of electron-hole pairs as well as to lead to luminescence emission far below the bulk band gap (quantum-confined Stark effect (QCSE), [47], [49]–[54]).

Another interesting feature of the piezoelectric effect in nitride heterostructures is its influence on transport process of carriers. HSU and WALUKIEWICZ [55] have just revealed that the piezoelectric fields induced in pseudomorphically grown AlGaN on GaN strongly affect the defect formation energy. It causes an increase in the defect concentration in the barrier. Additionally, the piezoelectric fields lower the height of the potential barrier at the heterojunction [56]. Both combined effects result in a very efficient transfer of electrons to the GaN well, which leads to a considerable increase in their 2D concentration [43], [55], [57]–[59].

Piezoelectric-related phenomena, however, proved to be considerably weaker or even almost absent under a high excitation level necessary to achieve a lasing population inversion. It was found in photoluminescence measurements of HANG-LEITER *et al.* [60] that the position of the stimulated emission peak in nitride QWs is directly a good measure of the real band-gap energy without any QCSE shift. They attributed this fact to an effective Coulomb screening of the piezoelectric field by injected carriers. Similar results were also reported by CHICHIBU *et al.* [61], [62], DOMEN *et al.* [63], and PAK and CHUANG [64].

4.2. Double-heterostructure nitride active regions

For epilayer thicknesses exceeding their critical thickness value d_{cr}, the interface contains extended regions of excellent lattice fit separated by regions of poor fit located, *e.g.*, at misfit dislocations [39]. In an idealized case of a structure without any other crystal defects, density N_m of misfit dislocation may be almost directly related to the lattice misfit f

$$N_m = \left(\frac{f}{a_{epi}}\right)^2 = L_m^{-2} \tag{7}$$

where L_m is the misfit dislocation separation. For the GaN/Al$_{0.1}$Ga$_{0.9}$N heterojunction, we found from Eq. (7) $N_m = 5.9 \cdot 10^9$ cm^{-2} at RT and $N_m = 6.0 \cdot 10^9$ cm^{-2} at 1020 K, the assumed growth temperature. In the calculations, we have assumed RT values [62] of the a lattice parameter to be equal to 0.31892 nm for GaN and to

0.31115 nm for AlN, their corresponding 1020-K values (calculated using thermal expansion coefficient given in [65] and [66] of 0.32020 nm and 0.31234 nm, respectively, and used the linear composition dependence of the a lattice constant in $Al_xGa_{1-x}N$ compounds.

An increase in density of mismatch-related centers of nonradiative recombination at heterojunctions is followed by a decrease in the device internal quantum efficiency η_1 which, assuming no other nonradiative mechanisms, reads as follows [67]:

$$\eta_1 = \left(1 + \frac{2S\tau_r}{d_A}\right)^{-1} \tag{8}$$

where τ_r is the radiative minority carrier lifetime and interface recombination velocity S (in cm/s) may be expressed by the following empirical relationship:

$$S \approx S_A f \tag{9}$$

where S_A is the proportional coefficient. Using approximately Eq. (8) (with $S_A = 2 \cdot 10^7$ originally determined for InGaAsP structures) for our $GaN/Al_{0.1}Ga_{0.9}N$ 0.2-μm DH active region, the values η_i as low as only about 10% are estimated for $\tau_r = 1.8$ ns [68] and about 6.5% for $\tau_r = 2.9$ ns [69], [70]. Taking into accout considerable reabsorption of laser radiation within resonators, the above values of internal quantum efficiencies η_i are in sharp contrast with reported values of external quantum efficiencies η_e achieved in Nichia InGaN/AlGaN DH light-emitting diodes (LEDs) which even exceeded 5% [71]. Also high-performance UV GaN/AlGaN DH LEDs [7]−[10] exhibit relatively high values η_e of over 1.5%. Taking into consideration a doubtless fact that dislocations act as nonradiative centres [72], [73] we have to conclude that there exist factors causing a decrease in dislocation densities N_D in nitride devices. In fact, RUVIMOV et al. [74] proved that Si doping improves the quality of nitride heterostructures reducing dislocation densities by about an order of magnitude. Doping atoms probably fill vacancies and reduce vacancy driven effects [75]. The above is also supported by observations of NAKAMURA et al. [76], who have considerably reduced threshold current densities of nitride EELs increasing Si doping in their active regions, and by photoluminescence (PL) measurements of PAKULA et al. [77], SCHUBERT et al [78], and CHO et al. [79], indicating an increase in the PL total intensity with an increase in silicon concentration. Therefore, the total dislocation density in GaN layers grown, *e.g.*, on (0001) sapphire with a GaN or AlN buffer layer may be as low as only in 10^8 cm^{-2} range [80] despite of a huge, over 13% lattice mismatch [39], [81]. Anyway, we still have to cope with huge dislocation densities in nitride structures although in high-quality silicon and arsenide semiconductors, dislocation densities as low as less than 0.1 cm^{-2} and 50 cm^{-2}, respectively, are routinely achieved [82].

The value of the parameter S_A has not been determined for nitride structures. Therefore, Eq. (8) cannot be used in more exact calculations. Fortunately, SUGAHARA et al. [35] have conducted a thorough study of dislocation-related influences on recombination phenomena in nitrides, assuming that the hole concentration near the dislocation is changing with a distance r from it proportional-

ly to $1-\exp(-r/L_p)$, where L_p is the hole diffusion length in the n-type GaN. Following their approach, we may present the internal quantum efficiency in the following form:

$$\eta_i = 1 - \left(\frac{2r_0}{L_D}\right)^2 - 8\left(\frac{L_p}{L_D}\right)\left[1 + \frac{r_0}{L_p} - \left(1 + \frac{L_D}{2L_p}\right)\exp\left(\frac{2r_0 - L_p}{2L_p}\right)\right] \quad (10)$$

where r_0 stands for the radius of a dark spot around a dislocation, and $L_D = N_D^{-1/2}$ is the mean dislocation separation. In Figure 2, we have plotted η_i as a function of the dislocation density N_D assuming $L_p = 50$ nm [73] and $r_0 = 50$ nm [35]. It is
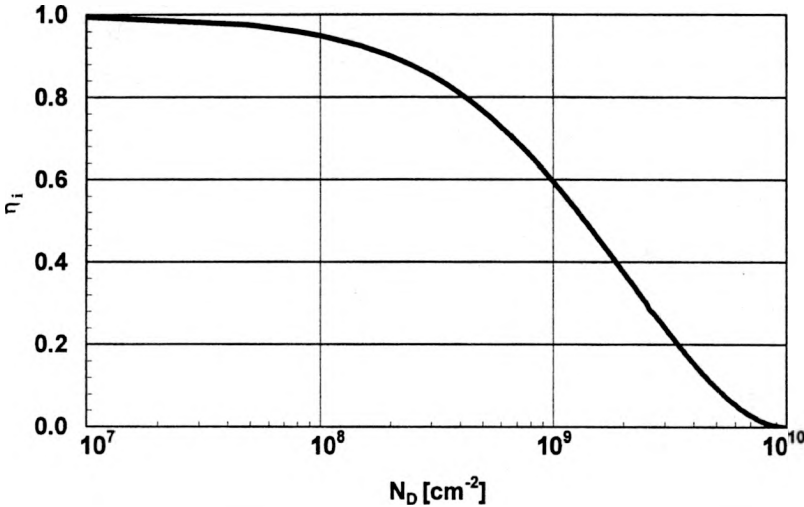

Fig. 2. Internal quantum efficiency η_i in a nitride active region as a function of the dislocation density N_D.

evident from the figure that to keep η_i over 90% value, dislocation densities inside nitride active regions should be reduced below $2\cdot10^8$ cm^{-2}, whereas their increase over $1\cdot10^{10}$ cm^{-2} excludes any rediative recombination. In our numerical calculations concerning QW nitride VCSELs, three values of N_D will be considered, as listed in Tab. 1. Only the last one, 10^9 cm^{-2}, is assumed for bulk DH nitride active regions because of additional misfit dislocations expected in their volumes. Additionally, in the last column of the table, scattering optical losses (*cf.* Eq. (2)) are shown, being assumed on the basis of results reported in [30].

T a b l e 1. Dislocation-related model parameters.

N_D [cm^{-2}]	η_i	α_{scatt} [cm^{-1}]
10^8	0.9500	1.5
$5\cdot10^8$	0.7670	7.5
10^9	0.5958	15.0

5. Results

In the simulation of pulsed-operated nitride VCSELs, all thermal phenomena are assumed to be negligible, which means that temperature throughout the device volume is assumed to be equal to the ambient one. From among all QWs, the 4-nm quantum well was found to give the lowest threshold current densities in SQW nitride VCSELs [36], [37], so only this QW width will be considered in all further threshold calculations concerning QW nitride VCSELs. For similar reasons, the typical bulk active-layer thickness, namely $d_A = 0.2$ μm, is assumed for DH nitride VCSELs on the basis of preliminary calculations. Reasonable (± 0.05 μm) changes of these thicknesses, however, were found not to have an essential impact on the results. In the case of MQW active layers, homogeneous injection of carriers in all QWs is assumed [83], so the cumulative thickness of the active region is just the sum of the thicknesses of all the individual active regions [38]. Unless distinctly indicated, values of the model parameters listed in Tab. 2 are used in the calculations.

T a b l e 2. Standard set of the model parameters.

Parameter	Notation	Value
Design wavelength	λ_0	370 nm
Active-region radius	r_A	5 μm
Active-region thickness (DH)	d_A	0.2 μm
Active-region thickness (SQW)	d_A	4 nm
Active-region thickness (MQW)	d_A	$M \cdot 4$ nm
Structure radius	r_S	50 μm
Spacer thicknesses	d_P, d_H	0.5 μm
Substrate thickness	s_{dub}	90 μm
Buffer thickness	d_{buff}	10 μm
Ambient temperature	RT	300 K

The threshold current density j_{th} (5) is directly connected with the threshold carrier concentration n_{th} determined using the lasing condition (1). Therefore j_{th} is directly associated with mirror reflectivities R_F and R_R deciding about the value of the end loss coefficient α_{end} (3). Let us first consider threshold of 4-nm SQW VCSELs. Plots of their threshold current densities j_{th} versus reflectivities of resonator mirrors for both the gain-guided (GG) and the index-guided (IG) configurations are presented in Fig. 3. The curves are plotted for three N_D values: 10^8 cm^{-2}, $5 \cdot 10^8$ cm^{-2} and 10^9 cm^{-2} (cf. Tab. 1). All curves demonstrate dramatic threshold increase with a decrease in mirror reflectivities below acceptable values, which depend on a VCSEL configuration and a dislocation density N_D. Like in the previous case, in arsenide and phosphide VCSELs, extremely high mirror reflectivities are necessary in order to obtain lasing. As one can see, an increase in N_D is followed by a rapid increase in lasing thresholds. For IG VCSELs with $R_F R_R = 99.9\%$ and successive N_D values, j_{th} is equal to 0.7 kA/cm^2, 1.8 kA/cm^2 and 6.5 kA/cm^2. A similar increase for GG VCSELs is even more dramatic: 3.0 kA/cm^2, 8.3 kA/cm^2 and 31.9 kA/cm^2
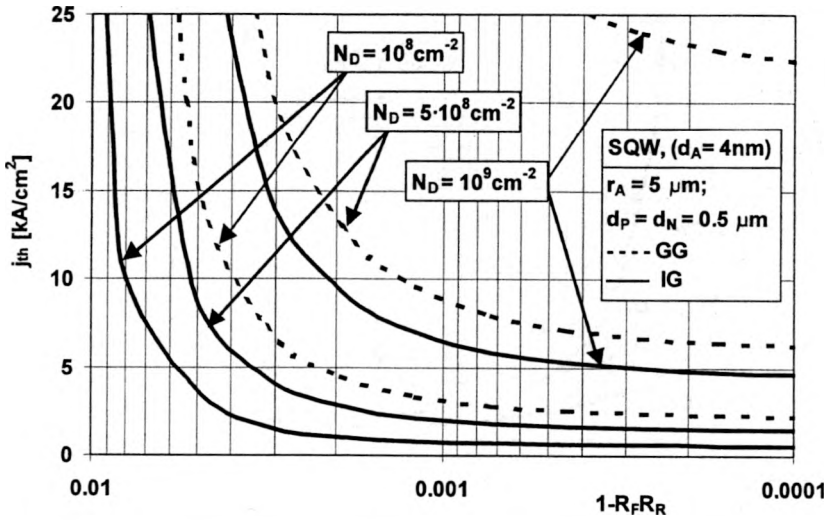
Fig. 3. Room-temperature pulse threshold current densities j_{th} of GG and IG 4-nm SQW GaN/AlGaN/AlN VCSELs versus a product $R_F R_R$ of reflectivities of their resonator mirrors plotted for three values of the dislocation densities N_D.

(not shown). For each N_D value, the IG structure ensures much lower thresholds than the GG one. In the case of relatively low dislocation density $N_D = 10^8$ cm^{-2}, for example, the threshold range below 10 kA/cm^2 is achieved for $R_F R_R > 99.6\%$ and for $R_F R_R > 99.2\%$ for the GG and the IG configurations, respectively. Analogous values for 5 kA/cm^2 are equal to 99.76% and 99.4%, respectively. The 2 kA/cm^2 threshold is still achieved for the IG structure (for $R_F R_R > 99.6\%$), but it is unattainable for the GG one.
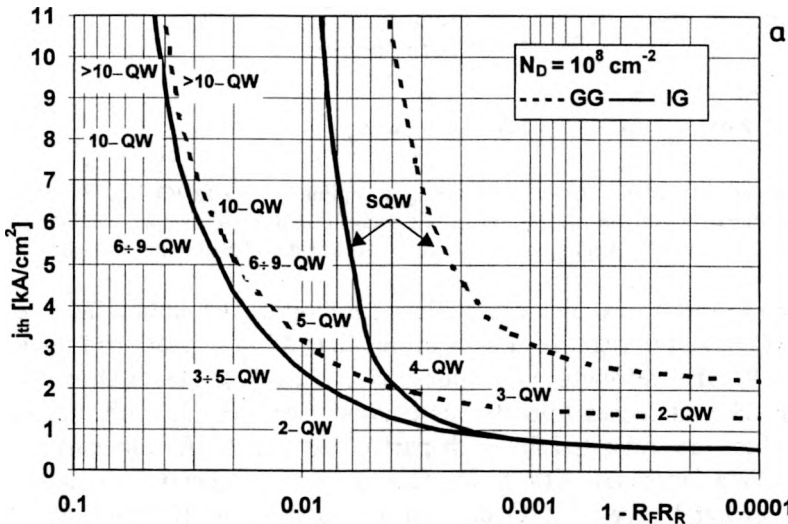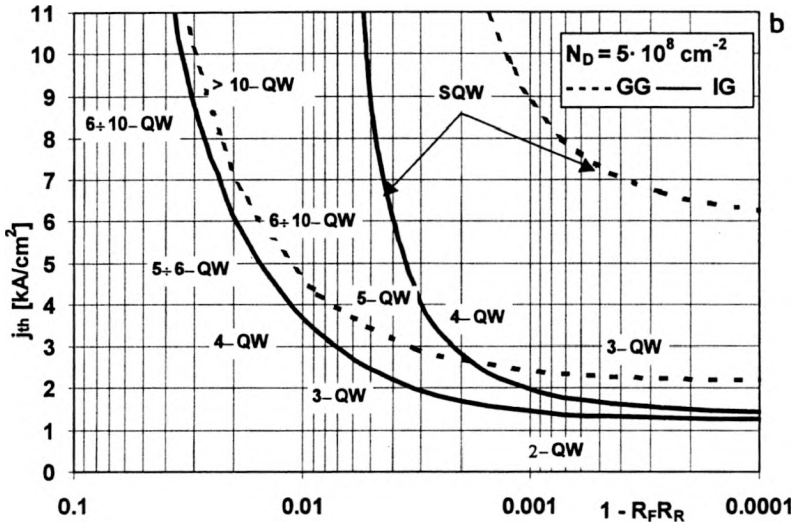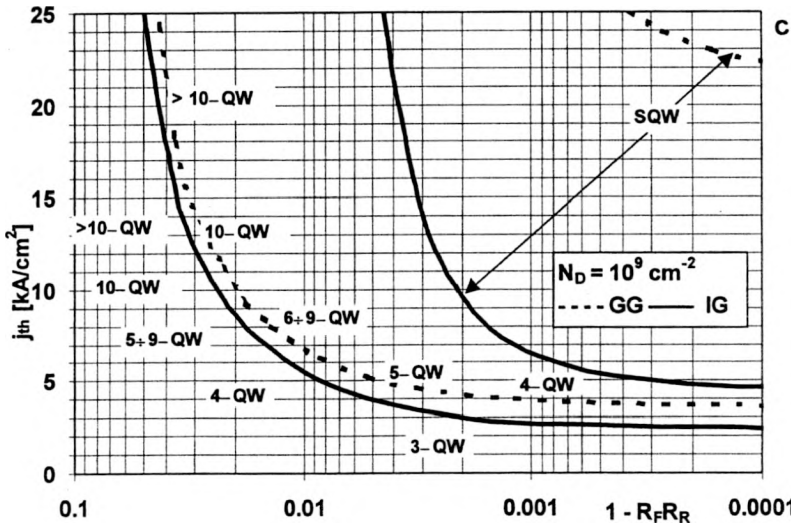

Fig. 4a

Fig. 4b

Fig. 4c

Fig. 4. Room-temperature pulse threshold current densities j_{th} of optimal GG and IG MQW nitride VCSELs versus resonator mirror reflectivities $R_F R_R$ plotted for dislocation densities N_D: a — 10^8 cm^{-2}, b — $5 \cdot 10^8$ cm^{-2}, and c — 10^9 cm^{-2}. Analogous plots for SQW nitride VCSELs are slso shown.

Assuming that the lowest thresholds are achieved for optimal numbers M_{opt} of quantum wells in MQW active regions, it was found that M_{opt} is proportional to total optical losses in VCSEL resonators. For successive N_D values, this is shown in Fig. 4a−c for changed end losses (directly associated (see Eq. (3) with mirror reflectivities). M_{opt} values are indicated for each part of the curves. As one can see, optimal number of QWs increases with a decrease in mirror reflectivities, being, however, always somewhat larger for GG configurations than for IG ones. So, if

there is a problem with manufacturing highly-relative resonator mirrors, MQW active regions containing many QWs are strongly recommended. For higher reflectivities, structures with a decreasing number of QWs seem to be optimal. In the case of extremely high mirror reflectivities, however not achievable using currently available technology, SQW nitride VCSELs would be the lowest-threshold nitride VCSELs.
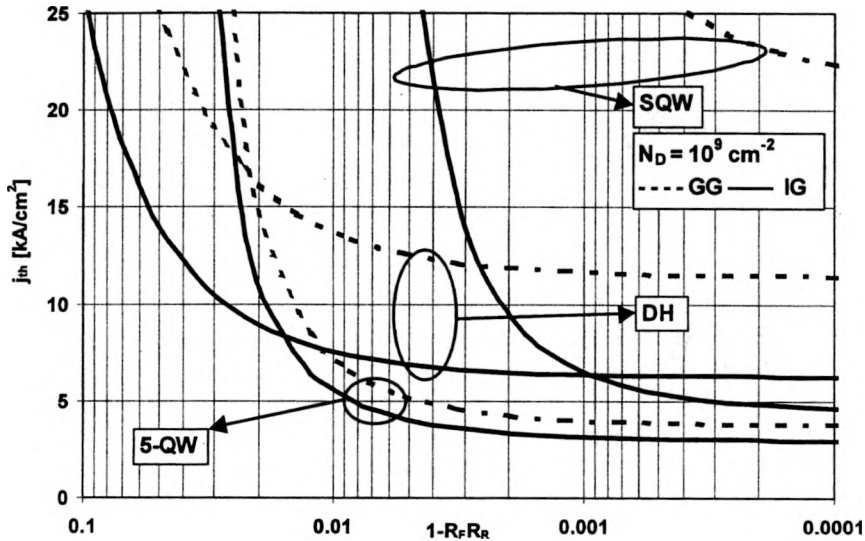

Fig. 5. Room-temperature pulse threshold current densities j_{th} of GG and IG configurations of SQW, 5-QW, and DH (bulk) nitride VCSELs versus resonator-mirror reflectivities determined for $N_D = 10^9$ cm^{-2}.

In Figure 5, a comparison between VCSEL structures with DH, SQW and 5-QW (MQW with 5 QWs) active regions is made for both their IG and GG configurations assuming the dislocation density $N_D = 10^9$ cm^{-2}. For very high mirror reflectivities, SQW index-guided VCSEL designs exhibit quite low thersholds, as expected, but still a little higher than those determined for both 5-QW VCSELs. The IG SQW thresholds, however, grow up very quickly with an increase in end losses (*i.e.*, with a decrease in a $R_F R_R$ product). While these thresholds are even lower than 5 kA/cm^2 for extremely high reflectivities of $R_F R_R > 99.97\%$, they are growing to as much as over 25 kA/cm^2 value for still very high $R_F R_R \approx 99.5\%$. On the other hand, GG SQW active regions cannot guarantee in this case low thresholds even for the highest mirror reflectivities. Both IG and GG configurations of 5-QW VCSELs ensure a very low threshold for relatively high reflectivities: it is lower than 5 kA/cm^2 for $R_F R_R > 99.2\%$ and for $R_F R_F > 99.5\%$, for IG and GG 5-QW VCSELs, respectively. For lower mirror reflectivities, however, both these thresholds exhibit a dramatic increase, exceeding the value of 25 kA/cm^2 for $R_F R_R \approx 97.2\%$ and 97.5\%, respectively.

Surprisingly, DH nitride VCSELs (*cf.* Fig. 5) are found to be much less sensitive to any increase in optical losses, including also end losses, than their QW counterparts. This leads us to an important conclusion that if there are problems with manufacturing nitride layers of sufficiently high quality (*i.e.*, low dislocation densities and low material absorption) as well as DBR mirrrors of sufficiently high reflectivities, simple DH nitride VCSELs may appear to be superior to QW ones. But unfortunately, their thresholds may then be still too high for efficient RT VCSEL operation.
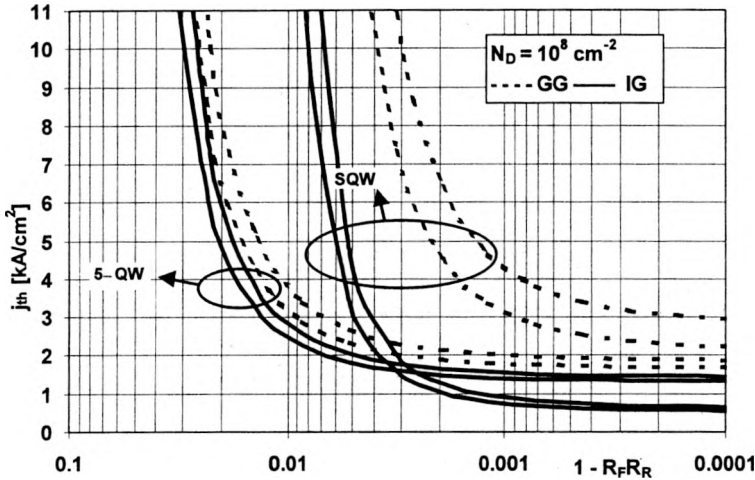

Fig. 6. Illustration of the stress impact on j_{th} versus $R_F R_R$ plots determined for GG and IG configurations of SQW and 5-QW nitride VCSELs for $N_D = 10^8$ cm^{-2}. For each pair of curves, the left-hand-side curve corresponds to the strain-included case.

Let us now reconsider the problem of strain-induced influence on optical gain in nitride QWs. Figure 6 shows threshold current densities j_{th} versus $R_F R_R$ plots determined for $N_D = 10^8$ cm^{-2} for SQW and 5-QW VCSELs. For each VCSEL design, a pair of curves is plotted, each of them shifted a little horizontally with respect to the other. The left-hand-side curve corresponds to the strain-included case, whereas the right-hand-side one is plotted without taking into account stress fields. The magnitude of the shift between both curves illustrates an impact of strain-related phenomena. As one can see, contrary to conventional arsenide and phosphide VCSELs, the influence of strain on thresholds of nitride QW VCSELs is much less significant (*cf.* [34], [42]), giving, however, always somewhat lower threshold when stress phenomenon is included.

6. Conclusions

A simple, but still detailed, analytical model is used to examine the influence of mismatch-related phenomena on a room-temperature operation of nitride VCSELs. An increase in the optical gain accomplished with the aid of intentionally intro-

duced strain in an active-region (band-gap engineering) is proved to be much less pronounced in nitride VCSELs than in conventional arsenide and phosphide VCSELs. Dislocation densities, on the other hand, have an essential harmful influence on VCSEL performance increasing scattering losses and decreasing internal quantum efficiency. A dislocation-related increase in threshold currents is especially sharp in the case of single-quantum-well nitride VCSELs and is steadily reduced with an increase in the number of quantum wells in multiple-quantum-well nitride VCSELs. Therefore, in the case of less advanced technology which cannot ensure low enough dislocation densities, higher numbers of quantum wells in active regions of nitride MQW VCSELs or even bulk double-heterostructure active regions are strongly recommended.

Until now, no electrically-pumped nitride VCSELs have been reported, which is justifiable considering their tough structure requirements. However, since the quality of nitride technology is being steadily improved, our hope is raised for launching in the near future research activities aiming at manufacturing these promising devices. Very recently, for example, a vertical injection light-emitting diode has been reported [84]. Its geometry resembles that of VCSELs. As the next step, designing of resonant-cavity nitride LEDs is predicted. So, nitride VCSELs may turn out to be than closer it has been generally thought.

Our simulation is intentionally developed in a simple mathematical form to give an easy tool for designing optimal structures of nitride VCSELs using only PC-level computing power. Because of the problems in finding exact values of some model parameters, results of this simulation should be considered only qualitatively. Nevertheless, they still enable the above important comparison between usabilities of different VCSEL structures, which was the main goal of this paper.

References

[1] STRITE S., MARKOÇ H. J., J. Vac. Sci. Technol. B **10** (1992), 1237.

[2] TERRIS B. D., MAMIN H. J., RUGAR D., Appl. Phys. Lett. **68** (1996), 141.

[3] NAKAMURA S., SENOH M., NAGAHAMA S., IWASA N., YAMADA T., MATSUSHITA T., KIYOKU H., SUGIMOTO Y., Jpn. J. Appl. Phys. (Pt. 2) **35** (1996), L74.

[4] KHAN M. A., OLSON D. T., VAN HOVE J. M., KUZNIA J. N., Appl. Phys. Lett. **58** (1991), 1515.

[5] REDWING J., LOEHER D. A. S., ANDERSON N. G., TISCHLER M. A., FLYNN J. S., Appl. Phys. Lett. **69** (1996), 1.

[6] NAKWASKI W., Opt. Quantum Electron. **28** (1996), 335.

[7] AKASAKI I., AMANO H., J. Electrochem. Soc. **141** (1994), 2266.

[8] HAN J., CRAWFORD M. H., Proc. SPIE **3419** (1998), 46.

[9] SAKHAROV A. V., LUNDIN W. V., USIKOV A., USHAKOV U. I., KUDRIAVTSEV YU. A., LUNEV A. V., SHERNIAKOV Y. M., LEDENTSOV N. N., MRS Internet J. Nitride Semicond. Res. **3** (1998), Artcle 28.

[10] HAN J., CRAWFORD H., SUHL R. J., FIGIEL J. J., BANAS M., ZHANG L., SONG Y. K., ZHOU H., NURMIKKO A. V., Appl. Phys. Lett. **73** (1998), 1688.

[11] SCHMIDT T. J., CHO Y.-H., SONG J. J., YANG W., Appl. Phys. Lett. **74** (1999), 245.

[12] PONCE F.A., BOUR D.P., GÖTZ W., JOHNSON N.M., HELAVA H.I., GRZEGORY I., JUN J., POROWSKI S., Appl. Phys. Let. **68** (1996), 917.

[13] NAKAMURA S., SENOH M., NAGAHAMA S., IWASA N., YAMADA T., MATSUSHITA T., KIYOKU H., SUGIMOTO Y., KOZAKI T., UMEMOTO H., SANO M., CHOCHO K., Appl. Phys. Lett. **72** (1998), 2014.

[14] POROWSKI S., MRS Internet, J. Nitride Semicond. Res. **4S1** (1999), Article G1.3.

[15] FOXON C.T., CHENG T. S., KORAKAKIS D., NOVIKOV S.N., CAMPION R.P., GRZEGORY I., POROWSKI S., ALBRECHT M., STRUNK H.P., MRS Internet, J. Nitride Semicond. Res. **4S1** (1999), Article G4.11.

[16] KAMP M., KIRCHNER C., SCWEGLER V., PELZMANN A., EBELING K.J., LESZCZYNSKI M., GRZEGORY I., SUSKI T., POROWSKI S., MRS Internet, J. Nitride Semicond. Res. **4S1** (1999), Article G10.2.

[17] AKASAKI I., AMANO H., KOIDE Y., HIRAMATSU K., SAWAKI N., J. Crys. Growth **98** (1989), 209.

[18] AMANO H., AKASAKI I., HIRAMATSU K., KOIDE N., SAWAKI N., Thin. Solid Films **163** (1988), 415.

[19] NAKAMURA S., SENOH M., MUKAI T., Jpn. J. Appl. Phys. **30** (1991), L1708.

[20] WEEKS T.W., BREMSER M.D., AILEY K.S., CARLSON E., PERRY W.G., DAVIS R.F., Appl. Phys. Lett. **67** (1995), 401.

[21] WEEKS T.W., BREMSER M.D., AILEY K.S., CARLSON E., PERRY W.G., PINER E.L., EL-MASRY N.A., DAVIS R.F., J. Mater. Res. **11** (1996), 1081.

[22] LUNDIN W.V., USIKOV A.S., PUSHNYI B.V., USHAKOV U.I., STEPANOV M.V., SCHMIDT N.M., SAKHAROV A.V., ZADIRANOV YU. M., SATURIN S.M., BUSOV V., Mater. Sci. Forum. **264** (1998), 1125.

[23] HIRAYAMA H., AOYAGI Y., MRS Internet, J. Nitride Semicond. Res. **4S1** (1999), Article G3.74.

[24] HONDA T., KAWANISHI H., SAKAGUCHI T., KOYAMA F., IGA K., MRS Internet, J. Nitride Semicond. Res. **4S1** (1999), Article G6.2.

[25] MROZIEWICZ B., BUGAJSKI M., NAKWASKI W., *Physics of Semiconductor Lasers*, North Holland, Amsterdam 1991, Chap. 4.1.9.

[26] BORN M., WOLF E., *Principles of Optics*, Pergamon Press, New York 1993, Sec. 1.6.5.

[27] BABIĆ D.I., CORZINE S.W., IEEE J. Quantum Electron. **28** (1992), 514.

[28] YOSHIDA S., MISAWA S., GONDA S., J. Appl. Phys. **53** (1982), 6844.

[29] PANKOVE J.I., BLOOM S., HARBEKE G., RCA Rev. **36** (1975), 163.

[30] LIAU Z.L., AGGARWAL R.L., MAKI P.A., MOLNAR R.J., WALPOLE J.N., WILLIAMSON R.C., MELNGAILIS I., Appl. Phys. Lett. **69** (1996), 1665.

[31] BABIĆ D.I., CHUNG Y., DAGLI N., BOWERS J.E., IEEE J. Quantum Electron. **29** (1993), 1950.

[32] HONDA T., KATSUBE A., SAKAGUCHI T., KOYAMA F., IGA K., Jpn. J. Appl. Phys. **34** (1995), 3527.

[33] MENEY A.T., O'REILLY E.P., Appl. Phys. Lett. **67** (1995), 3031.

[34] SUZUKI M., UENOYAMA T., J. Appl. Phys. **80** (1996), 6868.

[35] SUGAHARA T., SATO H., HAO M., NAOI Y., KURAI S., TOTTORI S.T., YAMASHITA K., NISHINO K., ROMANO L.T., SAKAI S., Jpn. J. Appl. Phys. (Pt.2) **37** (1998), L398.

[36] MAĆKOWIAK P., NAKWASKI W., Electron. Technology **30** (1997), 314.

[37] MAĆKOWIAK P., NAKWASKI W., J. Phys. D: Appl. Phys. **31** (1998), 2479.

[38] MAĆKOWIAK P., NAKWASKI W., MRS Internet, J. Nitride Semicond. Res. **3** (1998), Article 35.

[39] TRAMPERT A., BRANDT O., PLOOG K.H., *Gallium Nitride (GaN) I, Semiconductors and Semimetals*, Vol. 50, Academic Press, San Diego 1998, Chap. 7.

[40] AKASAKI I., AMANO H., Ref. [39], Chap. 15.

[41] AHN D., PARK S.-H., KIM T.I., IEEE J. Sel. Topics Quantum Electron. **4** (1998), 520.

[42] SUZUKI M., UENOYAMA T., Jpn. J. Appl. Phys. (Pt.1) **35** (1996), 1420.

[43] BYKHOVSKI A., GELMONT B., SHUR M., J. Appl. Phys. **74** (1993), 6734.

[44] BYKHOVSKI A.D., KAMINSKI V.V., SHUR M.S., CHEN Q.C., KHAN M.A., Appl. Phys. Lett. **68** (1996), 818.

[45] BERNARDINI F., FIORENTINI V., Phys. Rev. B **57** (1998), R9427.

[46] MAJEWSKI J.A., ZANDLER G., VOGL P., Semicond. Sci. Technol. **13** (1998), A90.

[47] MILLER D.A.B., CHEMLA D.S., DAMEN T.C., GOSSARD A.C., WIEGMANN W., WOOD T.H., BURRUS C.A., Phys. Rev. Lett. **53** (1984), 3173.

[48] TAKEUCHI T., WETZEL CH., YAMAGUCHI S., SAKAI H., AMANO H., AKASAKI I., KANEKO Y., NAKAGAWA S., YAMAOKA Y., YAMADA N., Appl. Phys. Lett. **73** (1998), 1691.

[49] CHICHIBU S.F., ABARE A.C., MINSKY M.S., KELLER S., FLEISCHNER S.B., BOWERS J.E., HU E., MISHRA U.K., COLDREN L.A., DENBAARS S.B., Appl. Phys. Lett. **73** (1998), 2006.

[50] MILLER D.A.B., CHEMLA D.S., DAMEN D.C., GOSSARD A.C., WIEGMANN W., WOOD T.H., BURRUS C.A., Phys. Rev. B **32** (1985), 1043.

[51] MILLER D.A.B., CHEMLA D.S., SCMITT-RINK S., Phys. Rev. B **33** (1986), 6976.

[52] SMITH D.L., MAILHIOT C., Phys. Rev. Lett. **58** (1987), 1264.

[53] TAKEUCHI T., TAKEUCHI H., SOTA S., SAKAI H., AMANO H., AKASAKI I., Jpn. J. Appl. Phys. (Pt. 2) **36** (1997), L177.

[54] TAKEUCHI T., SOTA S., KATSURAGAWA M., KOMORI M., TAKEUCHI H., AMANO H., AKASAKI I., Jpn. J. Appl. Phys. (Pt. 2) **36** (1997), L382.

[55] HSU L., WALUKIEWICZ W., Appl. Phys. Lett. **73** (1998), 339.

[56] UNDERWOOD R.D., KOZODOY P., KELLER S., DENBAARS S.P., MISHRA U.K., Appl. Phys. Lett. **73** (1998), 405.

[57] YU E.T., DANG X.Z., YU L.S., QIAO D., ASBECK P.M., LAU S.S., SULLIVAN G.J., BOUTROS K.S., REDWING J.M., Appl. Phys. Lett. **73** (1998), 1880.

[58] AMBACHER O., SMART J., SHEALY J.R., WEIMANN N.G., CHU K., MURPHY M., SHAFF W.J., EASTMAN L.F., DMITROV R., WITTMER L., STUTZMANN M., RIEGER W., HILSENBECK J., J. Appl. Phys. **85** (1999), 3222.

[59] RAMVALL P., AOYAGI Y., KURAMATA A., HACKE P., HORINO K., Appl. Phys. Lett. **74** (1999), 3866.

[60] HANGLEITER A., IM J.S., KOLLMER H., HEPPEL S., OFF J., SCHOLZ F., Internet J. Nitride Semicond. Research **3** (1998), Article 15.

[61] CHICHIBU S., SOTA T., WADA K., NAKAMURA S., J. Vac. Technol. B **16** (1998), 2204.

[62] CHICHIBU S., COHEN D.H., MACK M.P., ABARE A.C., KOZODOY P., MINSKY M., FLEISCHER S., KELLER S., BOWERS J.E., MISHRA U.K., COLDREN L.A., CLARKE D.R., DENBAARS S.P., Appl. Phys. Lett. **73** (1998), 496.

[63] DOMEN K., KURAMATA A., SOEJIMA R., HORINO K., KUBOTA S., TANAHASHI T., IEEE J. Sel. Topics Quantum Electron. 4 (1998), 490.

[64] PARK S.-H., CHUANG S.-L., Appl. Phys. Lett. **72** (1998), 3103.

[65] MOHHAMAD S.N., MARKOÇ H., Progress Quantum Electron. **20** (1996), No. 5/6.

[66] YIM W.M., PAFF R.J., J. Appl. Phys. **45** (1974), 1456.

[67] BEATS R., Solid-State Electron. **30** (1987), 1175.

[68] NAKAMURA S. IEEE J. Sel. Topics Quantum Electron. 4 (1998), 483.

[69] NAKAMURA S., FASOL G., *The Blue Laser Diode*, 1st edit., Springer-Verlag, Berlin 1997, p. 252.

[70] IM J.S., HAERLE V., SCHOLZ F., HANGLEITER A., MRS Internet J. Nitride Semicond. Research 1 (1996), Article 37.

[71] Reference [69], p. 198.

[72] FIGIELSKI T., Solid-State Electron. **21** (1978), 1403.

[73] HAO M., SUGAHARA T., TOTTORI S., NOZAKI M., KURAI S., NISHINO K., NAOI Y., SAKAI S., Proc. SPIE **3419** (Optoelectronic Materials and Devices) (1998), 138.

[74] RUVIMOV S., LILIENTAL-WEBER Z., SUSKI T., AGER III J.W., WASHBURN J., KRUEGER J., KISIELOWSKI C., WEBER E.R., AMANO H., AKASAKI I., Appl. Phys. Lett. **69** (1996), 990.

[75] MARKOÇ H., IEEE J. Sel. Topics Quantum Electron. 4 (1998), 537.

[76] NAKAMURA S., SENOH M., NAGAHAMA S., IWASA N., YAMADA T., MATSUSHITA T., SUGIMOTO Y., KIYOKO H., Appl. Phys. Lett. **70** (1997), 1417.

[77] PAKULA K., WOJDAK M., PALCZEWSKA M., SUCHANEK B., BARANOWSKI J.M., MRS Internet, J. Nitride Semicond. Research **3** (1998), Article 34.

[78] SCHUBERT E.F., GOEBFERT I.D., GRIESHABER W., REDWING J.M., Appl. Phys. Lett. **71** (1997), 921.

[79] CHO Y.-H., SONG J.J., KELLER S., MINSKY M.S., HU E., MISHRA U.K., DENBAARS S.P., Appl. Phys. Lett. **73** (1998), 1128.

[80] HAO M., SUGAHARA T., SATO H., MORISHIMA Y., NAOI Y., ROMANO L.T., SAKAI S., Jpn. Appl. Phys. (Pt. 2) **27** (1998), L291.

[81] MORKOÇ H., HAMDANI F., SALVADOR A., *Gallium Nitride (GaN) I, Semiconductors and Semimetals,* Vol. 50, Academic Press, San Diego 1998, Chap. 8.
[82] HERSEE S.D., RAMER J.C., MALLOY K.J., MRS Bulletin **22** (1997), 45.
[83] YEO Y.C., CHONG T.C., LI M.F., FAN W.J., J. Appl. Phys. **84** (1998), 1813.
[84] SONG Y.-K., DIAGNE M., ZHOU H., NURMIKKO A.V., CARTER-COMAN C., KERN R.S., KISH F.A., KRAMES M.R., Appl. Phys. Lett. **74** (1999), 3720.